CARBON 91 (2015) 188–199

Available at www.sciencedirect.com

ScienceDirect

journal homepage: www.elsevier.com/locate/carbon

SDS-stabilized graphene nanosheets for highly electrically conductive adhesives

Behnam Meschi Amoli [a,b,d], Josh Trinidad [a,b], Geoffrey Rivers [b,c], Serubbabel Sy [a,b], Paola Russo [b,c,d], Aping Yu [a,b], Norman Y. Zhou [b,c,d], Boxin Zhao [a,b,d,*]

[a] Department of Chemical Engineering, University of Waterloo, 200 University Avenue West, Waterloo, ON N2L 3G1, Canada
[b] Waterloo Institute for Nanotechnology, University of Waterloo, 200 University Avenue West, Waterloo, ON N2L 3G1, Canada
[c] Department of Mechanical and Mechatronics Engineering, University of Waterloo, 200 University Avenue West, Waterloo, ON N2L 3G1, Canada
[d] Center for Advanced Materials Joining, University of Waterloo, 200 University Avenue West, Waterloo, ON N2L 3G1, Canada

ARTICLE INFO

Article history:
Received 18 December 2014
Accepted 13 April 2015
Available online 20 April 2015

ABSTRACT

We report sodium dodecyl sulfate (SDS) stabilization of graphene nanosheets, with two different sizes as auxiliary fillers inside the conventional electrically conductive adhesive (ECA) composite. Using this non-covalent modification approach we were able to preserve the single-layer structure of graphene layers and prevent their re-stacking inside the composite, which resulted in a significant electrical conductivity improvement of ECAs at noticeably low filler content. Addition of 1.5 wt% small and large SDS-modified graphene into the conventional ECAs with 10 wt% silver flakes led to low electrical resistivity values of $5.5 \times 10^3\ \Omega$ cm and 35 Ω cm, respectively, while at least 40 wt% of silver flakes was required for the conventional ECA to be electrically conductive. A highly conductive ECA with very low bulk resistivity of $1.6 \times 10^{-5}\ \Omega$ cm was prepared by adding 1.5 wt% of SDS-modified large graphene into the conventional ECA with 80 wt% silver flakes which is less than that of eutectic lead-based solders.

1. Introduction

Electrically conductive adhesives (ECAs) are polymeric composites reinforced by conductive fillers ranging from metallic particles to carbon materials. These composites have drawn considerable attention as promising alternative materials for traditionally used toxic lead-based solders for a variety of applications such as light emitting diodes (LEDs) [1], liquid crystal displays (LCDs) [2], and electronic packaging [3] to resolve the environmental concerns, reduce the operating cost, provide finer pitch capability, etc [4].

To meet the minimum requirements for today's competing advanced electronic industries, ECAs are required to have high electrical conductivity at low filler content. The conventional ECAs (usually consist of epoxy and silver micro flakes) have low electrical conductivity even at high filler content, which jeopardizes their potential to replace lead-based solders for a wide variety of applications. Many efforts have been devoted to improving the electrical conductivity of ECAs at low silver content by introducing the nano-sized conductive fillers into the conventional formulation of ECAs [5–11]. A key parameter in electrical conductivity of an ECA is the

* *Corresponding author at:* Department of Chemical Engineering, University of Waterloo, 200 University Avenue West, Waterloo, ON N2L 3G1, Canada.
E-mail address: zhaob@uwaterloo.ca (B. Zhao).
http://dx.doi.org/10.1016/j.carbon.2015.04.039
0008-6223/

quality of the electrical network. The conductive nanofillers, depending on their type and morphology, affect the quality of network by influencing the contact resistance. The contact resistance is characterized by constriction resistances and tunnelling resistances [5]. It should be noted that the tunnelling resistance is a dominant parameter at low silver content [9,12]. It has been reported that the contact resistance can be remarkably reduced by introducing high aspect-ratio nanomaterials [13]. Many research groups have studied the effects of different high aspect-ratio nanomaterials such as silver nanowire (Ag NWs) [13,14], silver nanobelt (Ag NBs) [9], and carbon nanotubes (CNTs) [15,16] on the electrical properties of ECAs and reported the establishment of a percolated network at low silver content.

Recently, graphene, a flat monolayer of carbon atoms, densely packed into a honeycomb two-dimensional (2-D) lattice structure, has attracted great interest due to its exceptional electrical, thermal and mechanical properties [17–19]. Possessing the highest aspect-ratio and specific surface area among all the nanostructure materials, graphene can provide a more complete electrical network at lower filler content, making it a promising nanofiller for ECAs application [20]. Pu et al. used nitrogen-doped graphene inside the system of epoxy and silver powder and reported that the percolation of silver powder reduced to 30 wt% [21]. Their results confirmed that 2-D graphene is much more effective than other types of high aspect-ratio carbon-based fillers such as carbon nanotubes and carbon black. However, the challenge of attaining a homogeneous dispersion, as well as preserving its single-layer structure inside the composite acts as a bottleneck in ECA fabrication.

Surface modification of graphene using organic materials is one approach to exfoliate graphene in which the interaction occurs via either covalent bonding or via π–π stacking. Although this technique is shown to be effective to exfoliate graphene layers, it hinders their electrical properties because it disturbs the π-electrons delocalization of graphene surface [22–25]. The surface decoration of graphene with inorganic nanoparticles (NPs) such as Ag NPs is another approach that can effectively exfoliate graphene nanosheets [26]. Some research groups applied this idea into ECA applications and used the Ag NP-decorated graphene for the formulation of ECAs; they reported a positive effect of Ag NP-decorated graphene on the electrical conductivity of ECAs [20,27,28]. Based on our recent study, we believe that the improved electrical conductivity of ECAs via addition of Ag NP-decorated graphene is mainly because of the reduction of the tunnelling resistance; however, the increased number of contact points (due to the presence of Ag NPs on the graphene surface) may cancel out this positive effect [29]. We showed that to decrease the number of contact points sintering of NPs must occur which requires elevated curing temperatures (higher than 150 °C). We hypothesize the single layer graphene without metallic decoration is a better option as auxiliary filler for ECA application if a proper exfoliation technique is applied to preserve its single layer structure within the epoxy matrix.

In our current study, we used a simple surfactant-assisted approach (based on the use of an ionic surfactant, sodium dodecyl sulfate (SDS)) to stabilize graphene nanosheets and disperse them inside the conventional ECAs (consisting of epoxy and silver micro flakes). Although the production of surfactant-stabilized graphene from graphite powder has been reported in literature [30], it is the first time that we report direct stabilization of graphene to be used inside ECA composites. In this technique, graphene layers are exfoliated by the mechanical energy provided by bath or horn sonication, which breaks the van der Waals interactions between graphene layers. At the same time, surfactant molecules are adsorbed onto the graphene layers surface and prevent their re-stacking via steric repulsions [25,30,31] (see Fig. 1A). The main advantage of using this approach for ECAs application is that we are able to preserve the single layer structure of graphene and prevent their re-stacking inside the nanocomposite without disturbing its structure. The exfoliated graphene nanosheets can effectively bridge between separated silver flakes and provide more surface area for electron transportation inside the electrical network (as illustrated in Fig. 1B). To shed further light on the effect of graphene aspect-ratio, we used graphene nanosheets with two different sizes (1 μm, and 3–5 μm diameter) and applied the same SDS modification approach to exfoliate and disperse them inside the conventional ECAs. The electrical resistivities of the hybrid ECAs (with small and large SDS-modified graphenes) were measured at different silver contents and compared with those of conventional and hybrid ECAs with non-modified graphene. The effect of SDS modification on the curing behaviour of epoxy and the thermal stability of hybrid composite was also investigated.

2. Experiments and methods

2.1. *Large and small size graphenes and their SDS-stabilization*

Large size graphene was produced via reduction of graphene oxide (GrO) which was synthesized by modified Hummer's method [32,33]. Large graphite pellets with average sizes of 1 mm to 5 mm was used to produce GrO. The reduction of GrO to produce graphene was achieved by pre-heating of GrO in vacuum oven for 6 h followed by thermal annealing in a furnace (protected with Ar) at 900 °C for 10 min. This process ensures the total removal of the oxygen functionality and restoration of the graphitic surface, so that the highest electrical conductivity can be achieved for the resulted large size graphene. Small size graphene was purchased from ACS material (USA).

In order to modify the graphene surface with SDS, both large and small graphene powders were dispersed into a solution of SDS (Sigma–Aldrich, ⩾99.0%) and ethanol. The concentration of SDS in ethanol was 0.06 mol/L. Then, the solution was ultrasonicated using a low power sonic bath (Branson 2510R-MT) for 30 min. In order to remove the unbonded SDS, the graphene dispersion was washed four times by repeatedly dispersing in fresh ethanol and centrifugation at 8000 rpm for 10 min to remove the supernatant. The final solution was then filtered using a polycarbonate (PC) membrane (with a pore size of 400 nm) and dried overnight at room temperature in a vacuum oven.

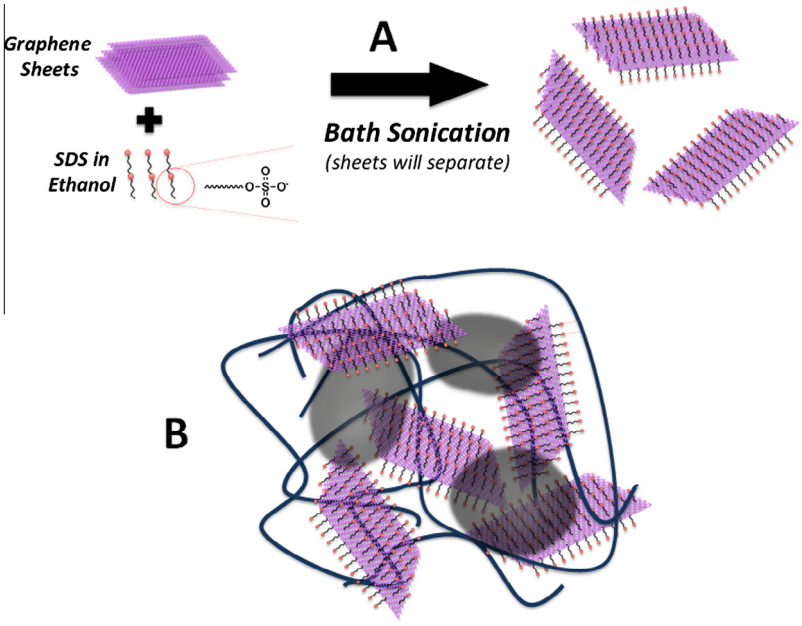

Fig. 1 – (A) SDS modification of graphene leads to exfoliation of graphene flakes; (B) the bridging of SDS-modified graphene between separated silver flakes establishes a compete electrical network inside epoxy. (A colour version of this figure can be viewed online.)

2.2. *Nanocomposite preparation*

Diglycidyl ether of bisphenol A epoxy (DER™ 322) and triethylenetetramine (TETA), supplied by DOW chemical company (USA), were used as the adhesive base and hardener, respectively. The weight ratio of hardener to epoxy was 0.13. Two general types of sample (conventional and hybrid ECAs) were prepared, as listed in Table 1. The conventional ECA contained only silver flakes (Aldrich, 10 μm) and epoxy, whereas the hybrid ECAs contained epoxy and a mixture of the graphene (either SDS-modified or non-modified) with silver flakes at different weight percent. To make a hybrid ECA with SDS-modified graphene (either small or large size), silver flakes were mixed with a dispersion of modified graphene in ethanol for 30 min and then epoxy was added to the mixture. The composite was mixed using the vortex mixer for one hour. In order to remove ethanol from the composite, the mixture was placed inside a desiccator and degassed in the consequent of 30 min followed by 5 min vortex mixing until ethanol was fairly removed (the final amount of in each composite type is shown in Table 2). Then the TETA was added to the mixture and the resultant paste was filled into a mold (7 mm × 7 mm × 0.5 mm) made using a glass slide and pieces of adhesive tape. A clean copper sheet was placed on top of the mold to ensure that the thickness of the sample remained constant, as well as to consistently produce a smooth surface. The samples were then pre-cured inside an oven at 60 °C for 30 min, and then cured at 150 °C for 2 h. After curing, the copper plate and the adhesive tape were removed. The schematic of nanocomposite preparation is presented in Fig. 2. A similar procedure was followed for the preparation of the hybrid ECA with non-modified graphene.

2.3. *Characterization methods*

Fourier Transform Infrared Spectroscopy (FTIR) (Tensor 27, Bruker Co.) analysis was carried out to confirm the SDS modification of graphene. A High Resolution Transmission Electron Microscope (HRTEM, JEOL 2010 F FEG) equipped with a field emission gun running at high resolution was used to determine the quality of exfoliation of graphene layers. The morphology of layers was investigated with an atomic force microscope (AFM) (Parks system NSOM model) in non-contact mode. Raman spectroscopy was performed using Bruker Senterra spectrometer (with 532 nm laser source). The bulk resistivity of ECAs and graphene pallets samples was tested

Table 1 – ECA samples and their conductive fillers.

Samples	Conductive filler system	Type of ECA
CCA	Silver flakes	Conventional ECA
HCA-SGS	Silver flakes and SDS-modified small graphene	Hybrid ECA
HCA-SGN	Silver flakes and non-modified small graphene	
HCA-LGS	Silver flakes and SDS-modified large graphene	
HCA-LGN	Silver flakes and non-modified large graphene	

Table 2 – Characteristic Cure and T_g data from DSC.

		Composition			
Name Description		Control 1 (Neat epoxy)	Control 2 (Ethanol diluted)	HCA-SGN	HCA-SGS
Ethanol content	PHR wt%	0 PHR 0 wt%	40.8 PHR 26.5 wt%	40.4 PHR 12.5 wt%	40.4 PHR 12.5 wt%
ΔH_{tot}	J/g	452.7	380.5	132.7	148.3
ΔH_{norm}	J/g_{matrix}	452.7	517.5	380.9	436.2
$T_{g\infty}$	°C	129.7	117.8	111.9	111.9

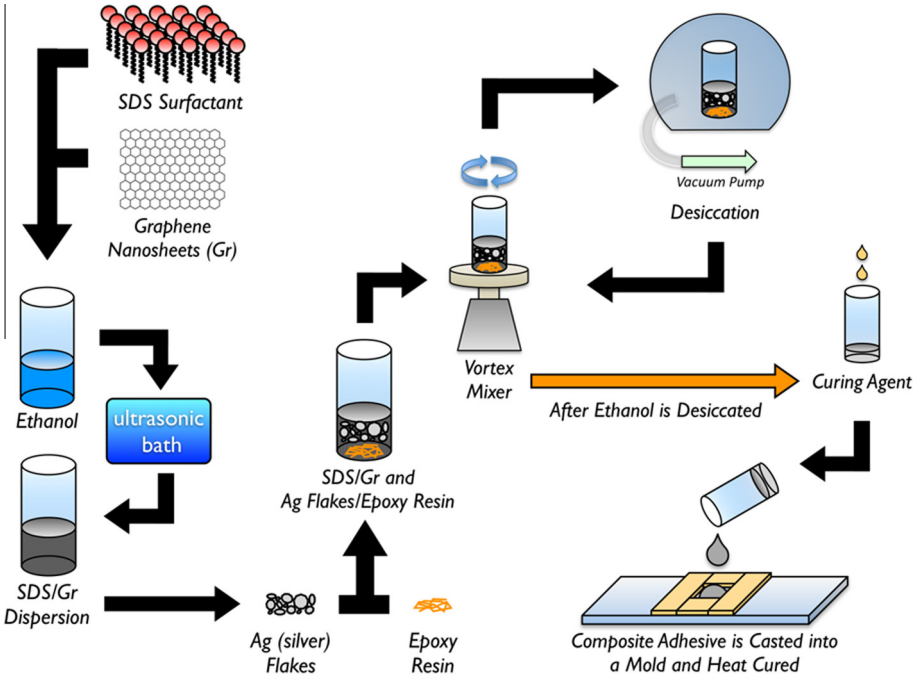

Fig. 2 – A schematic of a hybrid ECA nanocomposite preparation. (A colour version of this figure can be viewed online.)

through sheet resistance measurements using a four-point probe configuration. The setup is comprised of a probe unit (Cascade Microtech Inc.) and a source meter (Keithley 2440 5A Source meter, Keithley Instruments Inc.) The acquired sheet resistance was then converted into bulk resistivity using the following equation:

$$\rho = Ft\frac{\pi}{ln2}\left(\frac{V}{I}\right) \quad (1)$$

where F is a correction factor for samples with finite thicknesses, t is the sample thickness, I is the applied current and V is the voltage drop, measured by the source meter. The correction factor is defined as a function of the ratio of the sample thickness-to-probe spacing, denoted as s and so, for situations where the ratio between t and s is $0.4 < t/s < 1.0$, F can be approximated to 1 [29]. For our measurements, the sample thickness is ~0.5 mm and the spacing is 1 mm, therefore it is safe to assume that $F = 1$.

Using a Scanning Electron Microscope (SEM, LEO 1530, Carl Zeiss NTS), a study was carried out on the morphology of the electrical network inside the composites, as well as the filler–filler interaction between the graphene and the silver flakes. Differential Scanning Calorimetry (DSC) was performed for pure epoxy and composite to determine the rate of curing and their glass transition temperature (T_g). Polymer and composite DSC samples were encapsulated in hermetically sealed aluminum pans and cured during a 3 °C/min ramp to 180 °C in a TA4600 differential scanning calorimeter. The area under the exothermal peak was taken as the specific cure reaction enthalpy (ΔH_{tot}), in accordance with ASTM E2160-04. Samples were then cooled to 50 °C at 3 °C/min, and a second-heating scan performed to 180 °C using a modulation of ±0.477 °C every 60 s and an underlying heating rate of 3 °C/min. The glass transition temperature (T_g) of polymer and composite samples was determined from the reversing heat capacity ($Rev\ C_p$) signal of the second scan, using the methodology described by ASTM D7426-08. No residual cure signal was observed, confirming completion of the detectable enthalpic cure in the first heating scan [34]. Samples were then cooled to 50 °C at 3 °C/min before post-curing. Polymer

and composite samples were post-cured using heat-treatment cycles, applied by DSC. Each cycle consisted of heating the sample to 150 °C with an underlying heating rate of 3 °C/min, holding isothermally for 60 min, then cooling to 50 °C at 3 °C/min. Heating was modulated at ±0.477 °C amplitude every 60 s to obtain the reversing *Cp* component of the signal, determining the T_g at the beginning of each post-cure cycle. The $T_{g\infty}$ value reported is the value obtained when T_g stopped changing significantly between post-cure cycles, indicating post-cure was complete. Each sample was cycled 10 times to ensure that they reached a completely post-cured state. The thermogravimetric Analysis (TGA, TA instruments Q5000-1254) was used to study the thermal stability of the nanocomposites. Approximate 10 mg samples were placed in the TGA sample pan. Dynamic scan was performed from 40 to 800 °C with a heating rate of 10 °C/min under nitrogen atmosphere.

3. Results and discussion

Considering that the two types of graphene are from different sources, we first studied and compared their surface chemistry, defect contents, thickness, and even their intrinsic electrical conductivity so that we are able to draw a fair comparison when they are employed as auxiliary fillers inside the ECA. First, FTIR spectroscopy was performed for both types of graphenes to examine if there is any significant difference between their surface chemistry. As can be seen in Fig. S1, both of the small and large graphenes have similar FTIR spectra. More specifically, for both of them, the most characteristic peaks belong to C=C and C=O bonds, as highlighted by red dashed square. The FTIR results indicate there is no significant difference between the surface functional groups of the as-prepared small and large graphenes.

Raman spectroscopy was also carried out for these two types of graphene to examine the content of defects on their surface. The defect content is indicated by the ratio of the intensity of the D band (~1350 cm^{-1}) to the intensity of the G band (~1580 cm^{-1}), defined as I_D/I_G ratio [30]. As can be observed in Fig. S2, both of the small and large graphenes have almost the same I_D/I_G ratio (~0.96), indicating similar surface quality between the two graphene.

AFM was also performed to compare the thickness of these graphenes before SDS treatment. Figs. S3A and S3B show the images of non-modified small and large graphenes, and Figs. S3D and S3E present their relative height profile, respectively. It can be noticed that the step between the substrate and the layers of large graphene is ~7 nm, as the average value found for the small non-modified graphene (~6–7 nm). These values may denote that approximately 10 layers of graphene stacked together, as others reported 1–2 nm height for single layer graphene [20]. Representative SEM images of small and large graphenes are shown in Fig. S4, indicating similarity in their crumpled morphology. The bulk resistivity of the compressed pallets of the small graphenes prior to SDS modification was measured and compared to that of large graphene (Fig. S5). The inserted image shows an optical image of a typical pallet which was used for the electrical conductivity measurements of the graphenes. The results showed that the bulk resistivities of both small and large graphenes (0.088 Ω.cm compared to 0.091 Ω cm, respectively) are in the same range with a slight difference.

To verify the adsorption of SDS on graphene layer surface, the FTIR was performed for pure SDS, non-modified graphene, and the SDS-modified graphene; the results are shown in Fig. 3. To make sure there was no un-bonded SDS left in the system, the mixture of SDS and graphene after sonication was vigorously washed with fresh ethanol using sonication and centrifugation. In the FTIR spectrum of non-modified graphene, the peaks at 1589 cm^{-1} and 1740 cm^{-1} are related to the stretching vibration of C=C and C=O bands, respectively [35]. Both of these peaks can be seen in the spectrum of SDS-modified graphene with slightly reduced intensities. Also, the peak at 1240 cm^{-1} in the spectrum of non-modified graphene is considered to be C–H in plane bending [36]. This peak is too weak and in the most cases cannot be seen, as it was diminished in the spectrum of the SDS-modified graphene. The spectrum of pure SDS shows peaks at 1248 cm^{-1}, 1219 cm^{-1}, and 1084 cm^{-1} which correspond to asymmetric and symmetric stretching modes of SO_4^{-2}, respectively. Furthermore, pure SDS spectrum shows CH_3 asymmetric, symmetric (2955 cm^{-1}, 2873 cm^{-1}) and CH_2 asymmetric, symmetric (2917 cm^{-1}, 2850 cm^{-1}) stretching vibrational frequencies [37]. The same peaks are observed in the spectrum of SDS-modified graphene (as highlighted in red and green), implying the presence of SDS on the graphene surface even after multiple vigorous washing cycles. These results confirm that graphene layers have been successfully stabilized with SDS.

TEM was carried out to examine the effectiveness of SDS modification on exfoliation of both small and large graphenes. The transparency of flakes to the electron beam implies the level of exfoliation [30]. The number of graphene layers can be indicated by counting the number of distinguishable edges in TEM images [38]. Fig. 4A and B are representative TEM images of non-modified and SDS-modified small graphene, respectively. The opaque feature of non-modified graphene implies the stacking of graphene layers which hindered the electron beam to pass through the sample. However, after SDS modification, we see a bright and transparent graphene layer with a single distinguishable edge. The HRTEM image of the red square-marked area of Fig. 4B clearly shows that the graphene layers are exfoliated to individual layers. Electron diffraction (ED) pattern of black square-marked area also confirms the single layer feature of the selected area, as the inner set of spots are more intense than the secondary set [38,39]. The blurry ring in the ED pattern is attributed to the amorphous structure of SDS covering the graphene surface. A representative TEM image of non-modified large graphene flakes is shown in Fig. 4C which have a similar dark structure as small graphene. However, as can be seen in Fig. 4D, after SDS treatment, the large graphene flake is transparent to the electron beams. The HRTEM image of the red square-marked area of Fig. 4D also shows there is only a single layer at the edge of the large flake.

We used the TEM images to analyze the effect of SDS modification on the lateral size of graphene. The end-to-end diagonal size of 20 flakes of both the small and large graphene before and after SDS treatment was measured. The average number for each case is shown in Fig. 4E. As can be observed

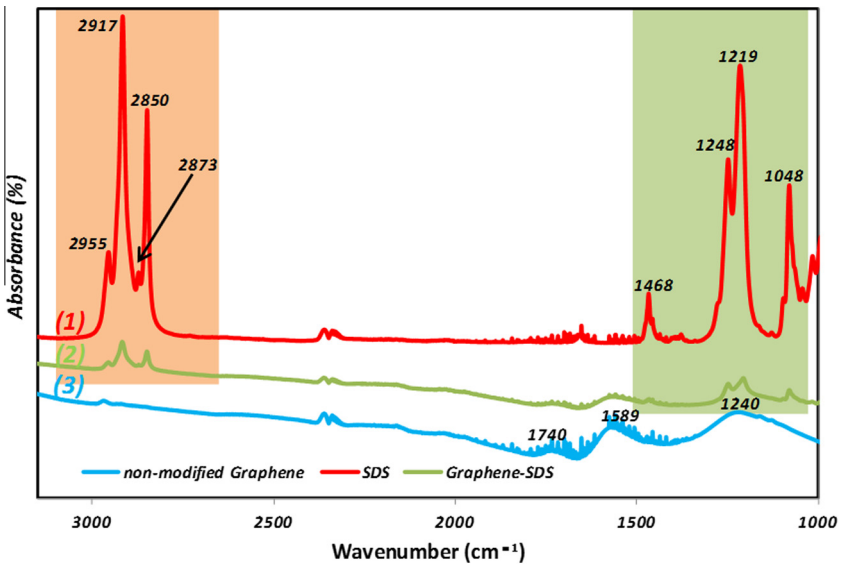

Fig. 3 – FTIR spectra of pure SDS (1), SDS-modified graphene (2), and non-modified graphene (3). (A colour version of this figure can be viewed online.)

in this figure, the diagonal sizes of SDS-stabilized small graphenes were always bigger than those of the non-modified ones. For the large graphene, the diagonal size difference was more evident. One explanation for the observed bigger size of the SDS-stabilized graphene compared to that of the graphenes before modification could be that there might be less folding for the SDS-modified graphene on the TEM grid, hence, giving a larger diagonal size. Overall, it is safe to conclude that the SDS modification did not reduce the size of the graphene layer.

To further study the effect of SDS modification on the structural properties of graphene, Raman spectroscopy was performed for the small graphene before and after SDS treatment to determine if the SDS treatment causes any additional defect to the structure of graphene. The results, presented in Fig. 5, are representative Raman spectra of small non-modified graphene and SDS-stabilized small graphene. As shown in Fig. 5A, the intensity of the G and D bands for both the non-modified and SDS-stabilized graphenes was in the same range. Comparison between I_D/I_G ratios of small graphene before and after SDS modification (0.963 and 0.959, respectively) indicates that the SDS modification did not disturb the chemical structure of graphene.

AFM was performed for small graphene before and after treatment to study the effect of SDS modification on the thickness of graphene layers. Figs. S3A and S3C show the AFM image of the non-modified small graphene and SDS-stabilized small graphene, respectively. Figs. S3D and S3F also show their relative height profiles, respectively. As mentioned earlier, it is possible to notice that small graphene layers are stacked together, leading to a multilayer structure. In particular, the height profile of Fig. S3A (displayed in Fig. S3D) shows a step between the substrate and the layer of 6.53 nm, which can be associated to the presence of approximately 10 layers of stacked graphene [20]. Graphene layers tend to re-stack together in solution and this is the reason why we found values around 6–7 nm for the thickness of non-modified graphene. The height profile of SDS-stabilized graphene (Fig. S3F) shows a step of 3.03 nm between the substrate and the first layer and a step of 3.03 nm between two consecutive layers. As expected, upon modification of the graphene layers with SDS, a better exfoliation of the material was achieved (see Fig. S3C). One may think that the value of 3.03 nm is far to be identified as single layer graphene, but it should be considered that the presence of the SDS on the graphene surface could lead to an overestimation of the thickness. The step of 3.03 nm could be attributed to the SDS molecules adsorbed on a single layer graphene sheet which is in the agreement with the observations of others [20]. Also, it should be noted that the graphene is easy to bend on AFM substrate leading to overestimated height profile.

Before adding graphene into the ECA formulation, the effect of SDS modification on the electrical properties of graphene was examined by measuring the bulk resistivity of small graphene pallets before and after the SDS treatment. As expected and can be seen in Fig. S5, the SDS modification of graphene increased the resistivity of graphene pallets because of the insulating layer of SDS. Note that even though the SDS-modified graphene has lower electrical conductivity, the electrical conductivity of the ECA filled the SDS-modified graphene is higher than that of the ECA with non-modified graphene, indicating the importance of stabilizing graphene inside ECA formulation.

To investigate the effectiveness of the SDS modification of graphene on enhancing the electrical conductivity and reducing the total silver content of hybrid ECAs, SDS-modified small graphene (1.5 wt%) was added into the conventional formulation of ECAs (denoted as CCAs) as a conductive co-filler to produce a customized hybrid ECAs (denoted as HCAs). The effect of SDS on electrical conductivity of ECAs was investigated by comparing the bulk resistivity of HCAs containing SDS-modified small graphene (denoted as HCA-SGSs) to that of HCAs with non-modified graphene (denoted as HCA-SGNs). The electrical resistivities of both the CCA and the

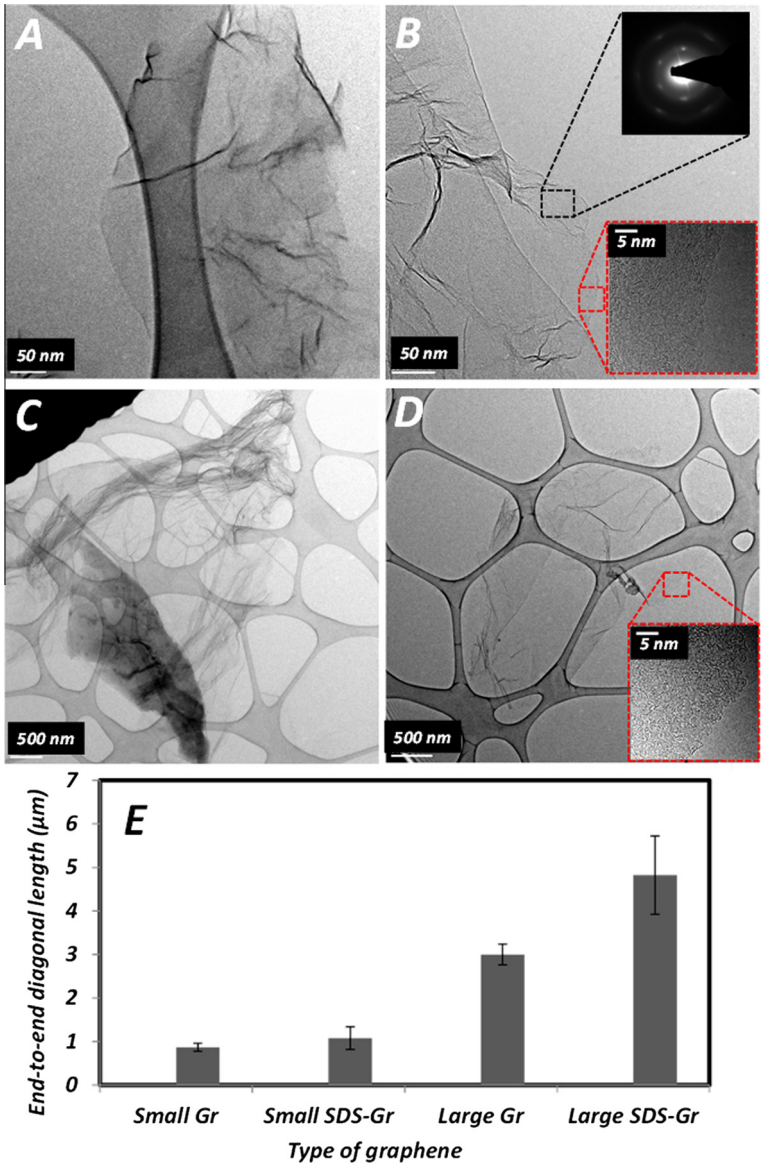

Fig. 4 – (A) a representative TEM image of a non-modified small graphene; (B) a representative TEM image of SDS-stabilized small graphene, the black inset is an electron diffraction pattern of the black marked area, the red inset is a HRTEM image of the red marked area of graphene edge; (C) a representative TEM image of a non-modified large graphene flake; (D) a representative TEM image of SDS-stabilized large graphene, the red inset is a HRTEM image of the red marked area of graphene edge, (E) the end-to-end diagonal size of small and large graphenes before and after SDS modification. (A colour version of this figure can be viewed online.)

HCA-SGNs at silver flakes contents less than 30 wt% were higher than the upper limit of our four-probe electrometer while a relatively low electrical resistivity of 0.4 Ω cm was achieved for HCA-SGSs at 30 wt% silver flakes. As can be seen in Fig. 6A, the percolation threshold for both the CCAs and the HCA-SGNs was 40 wt%, although the HCA-SGNs rendered lower bulk resistivity compared to the conventional ECAs. The lower bulk resistivity of the HCA-SGNs is because of the bridging effect of the graphene layers between the silver flakes. However, for HCA-SGS composites the percolation threshold was decreased to 10 wt%. This significant reduction in percolation content indicates the effectiveness of SDS to exfoliate and stabilize the graphene sheet inside the composite. The SDS modification of graphene provides the opportunity to fully take advantage of its high aspect-ratio which is crucial for decreasing the tunnelling resistance by bridging between separated silver flakes. It should be noted that a low bulk resistivity of 3×10^{-5} Ω cm was achieved for the HCA-SGS with 80 wt% silver flakes and 1.5 wt% SDS-modified graphene, showing one order of magnitude electrical conductivity improvement compared to CCA with the same silver flakes content.

Although we showed that the SDS-modified graphene improves the electrical conductivity of the hybrid ECAs, exceeding the optimal nanofiller concentration may hinder its positive performance. Hence, to investigate the effect of

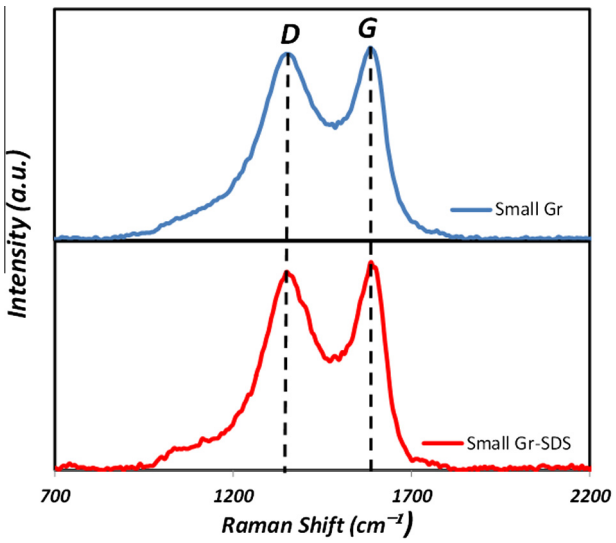

Fig. 5 – The Raman spectra of small graphene before and after SDS treatment. (A colour version of this figure can be viewed online.)

graphene concentration on the electrical conductivity of hybrid ECAs, SDS-modified graphene of varying concentrations were added into the CCAs and the bulk resistivity of the HCA-SGSs were measured. The same ranges of graphene concentrations were applied for CCAs with different silver concentrations to identify the optimal graphene content at each silver concentration (see Fig. 6B). The optimum graphene content was 1 wt% for the HCA-SGSs with 50 and 60 wt% of silver flakes while that concentration was 1.5 wt% for the HCA-SGSs with 70 and 80 wt% of silver flakes, indicating the importance of the weight ratio between silver micro flakes and graphene nanosheets on the electrical performance of HCAs. The increased bulk resistivity of the HCA-SGSs after the optimum concentration may attribute to the agglomeration of graphene at higher concentration. The dashed lines of Fig. 6B show the bulk resistivity of the HCA-SGNs at 60 and 80 wt% of silver flakes. The higher bulk resistivity of these samples compared to the HCA-SGSs with the same filler content is in agreement with our previous discussion on the positive effect of SDS treatment on the electrical conductivity of ECAs.

We demonstrated that the graphene with a proper surface functionality is a promising nanofiller to reduce the amount of silver flakes because of its high aspect-ratio. To shed further light on the relative significances of the graphene size (or aspect-ratio) and the surface functionality, another set of hybrid ECAs were produced using large graphene (3–5 μm in diameter) in contrast to the small graphene (1 μm in diameter), either unmodified or modified with SDS (HCA-LGN and HCA-LGS, respectively). Fig. 7 presents the bulk resistivity of these, in comparison with those of HCA-SGSs with comparable silver contents. As can be observed in Fig. 7, the bulk resistivity of the HCA-LGSs is noticeably lower than that of the HCA-SGSs, especially at low silver concentrations, when the silver flakes would be separated and rarely in direct contact. This demonstrates that when either are well distributed by SDS modification, the large graphene sheets are better able

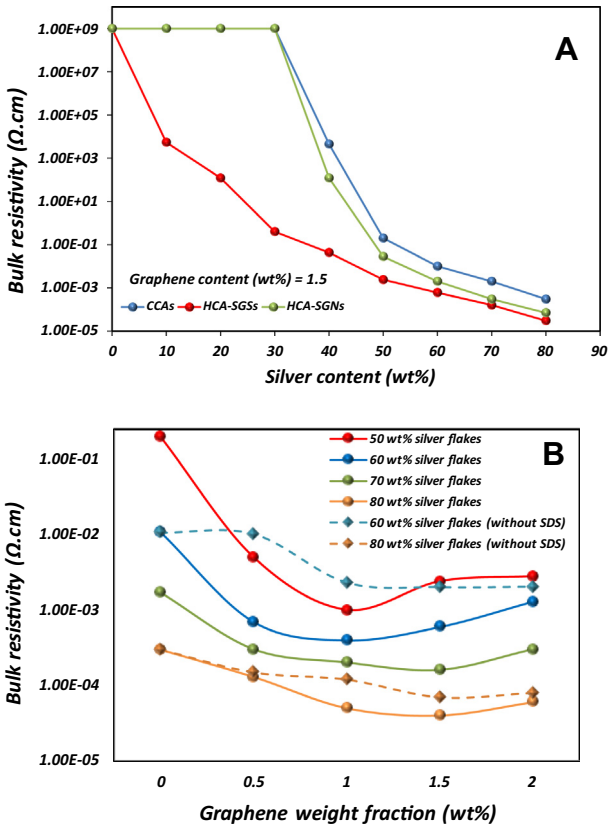

Fig. 6 – (A) Bulk resistivity of conventional ECAs (CCAs), hybrid ECAs with non-modified small graphene (HCA-SGNs), and hybrid ECAs with SDS-modified small graphene (HCA-SGSs), (B) the effect of SDS-modified small graphene concentration on the bulk resistivity of hybrid ECAs with different silver contents. (A colour version of this figure can be viewed online.)

to bridge the gaps between the silver flakes than the small graphene sheets, allowing further reductions in silver content. Addition of 1.5 wt% of large SDS-modified graphene into CCAs with 10 wt%, 20 wt%, and 30 wt% led to bulk resistivities

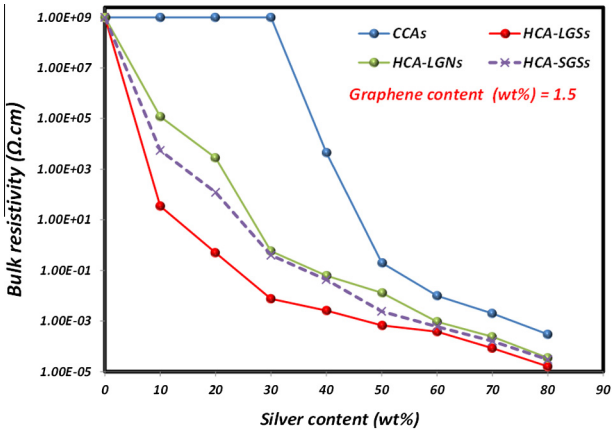

Fig. 7 – The effect of the size of graphene on the electrical conductivity of ECAs. (A colour version of this figure can be viewed online.)

of 35 Ω cm, 0.5 Ω cm, and 7.6×10^{-3} Ω cm, respectively, while those resistivities for the HCA-SGSs were 5.5×10^{3} Ω cm, 122 Ω cm, and 0.4 Ω cm, respectively. Fig. 7 also confirms the effectiveness of SDS in improving the electrical conductivity of the hybrid ECAs. Although the bulk resistivity of the HCA-LGNs was lower than that of the CCAs in all the silver content, those resistivity values were higher than those of HCA-LGSs. It should be noted that a highly conductive ECA with a very low electrical resistivity of 1.6×10^{-5} Ω cm was prepared by adding 1.5 wt% of SDS-modified large graphene into the CCA with 80 wt% of silver flakes. This bulk resistivity is even lower than that of eutectic lead-based solders [40]. Fig. 6 also shows that the electrical resistivity of HCA-LGNs is higher than that of HCA-SGSs in all the silver contents, indicating that the SDS modification effect might be more dominant in electrical conductivity improvement of ECAs than the effect of the aspect-ratio of conductive fillers.

To understand the mechanism of electrical conductivity improvement via addition of SDS-modified graphene, we performed SEM imaging to compare the quality of filler-filler interactions for the system of CCA, HCA-SGS, HCA-LGS, and HCA-LGN composites with 30 wt% silver flakes, as shown in Figs. 8A–D, respectively. For the hybrid ECAs, the concentration of graphene was 1.5 wt%. As can be observed in Fig. 8A, a large portion of silver flakes are separated by epoxy resin and the electrical network is not fully formed, as evidenced by electrical resistivity measurements (see Fig. 6A). However, the high aspect-ratio of graphene nanosheets helps to construct new electrical pathways for electron transportation inside the network. The yellow arrows of Fig. 8B identify small SDS-modified graphene sheets, spanning the gaps between separated flakes to form a connected network. As can be seen in this figure, the small graphene layers were reasonably dispersed inside the epoxy and no noticeable form of aggregation of graphene was observed. Fig. 8C also shows large SDS-modified graphene well dispersed inside epoxy. Because of the large size of graphene nanosheets more parts of the composite are covered by a conductive material. The yellow arrows of Fig. 8C representatively indicate a conductive path inside the conductive composite. Finally, Fig. 7D shows the SEM image of the HCA-LGN. As can be seen in this figure, the large graphene was not well dispersed inside the composite and large graphitic agglomerates formed, which explains the higher electrical resistivity of this type of ECA compared to that with SDS-modified graphene.

DSC was performed to study the effect of graphene SDS modification on the curing behaviour of epoxy as well as the T_g of the final nanocomposites. Characteristic DSC data is presented in Table 2, collected from the cure and post cure of two control group samples and two graphene composites (HCA-SGN and HCA-SGS). The control group samples are pure epoxy, and epoxy diluted with the same solvent content as the two nanocomposites. ΔH_{norm} represents the reported enthalpy normalized to only the mass of the hardened epoxy matrix [8]. Solvent masses for each composition have been presented using both the ethanol wt% in the total composite and the ethanol PHR (part per hundred resin mass as

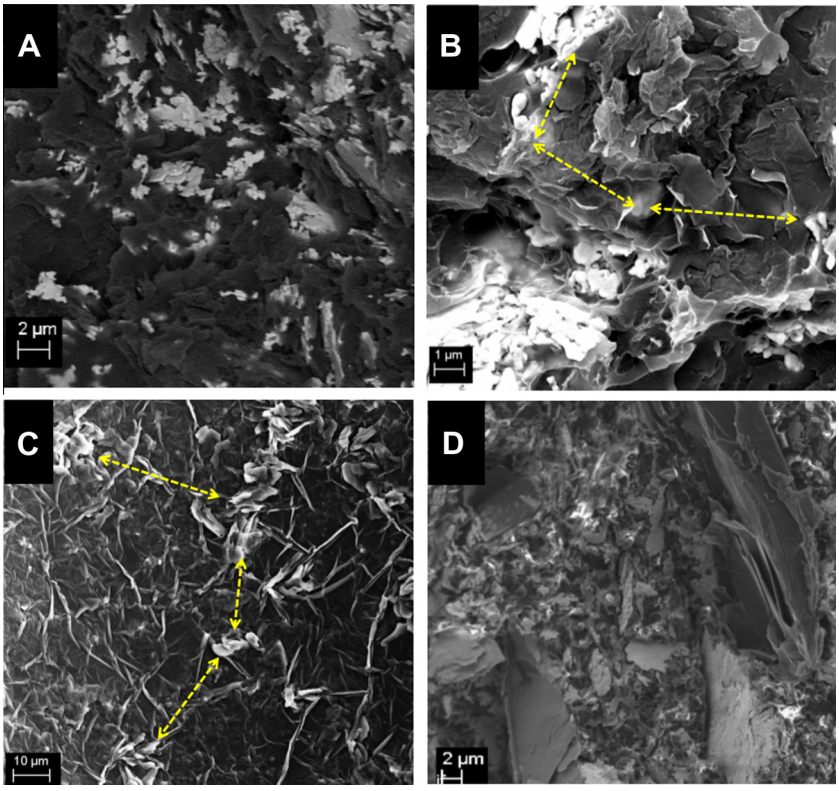

Fig. 8 – (A) a representative SEM image of the conventional ECA; (B) a representative SEM image of the hybrid ECAs with 1.5 wt% of SDS-modified small graphene; (C) a representative SEM image of the hybrid ECA with 1.5 wt% of SDS-modified large graphene; (D) and a representative SEM image of the hybrid ECA with 1.5 wt% of non-modified large graphene. Note: for all the ECAs the content of silver flakes was 30 wt%. (A colour version of this figure can be viewed online.)

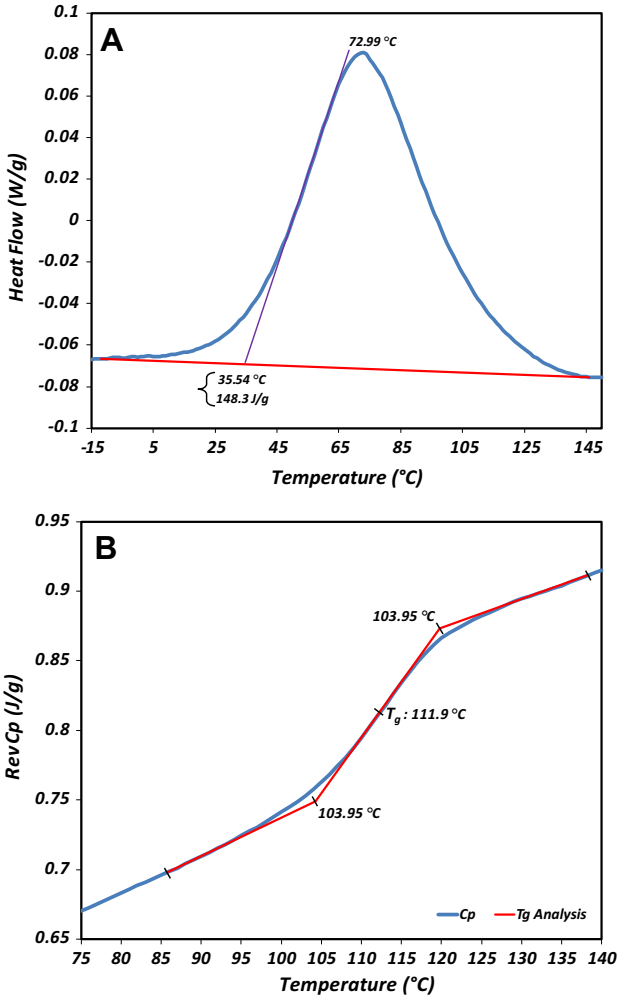

Fig. 9 – DSC data for HCA-SGS, demonstrating methods by which characteristic data was determined for (A) composite cure from heat flow and (B) composite T_g from Reversing *Cp*. Each trace was performed at 3 °C/min underlying heating rate. Modulation of ±0.477 °C every 60 s used in (B) only. (A colour version of this figure can be viewed online.)

reference), referencing the amount of ethanol present after degassing and at the start of curing. DSC traces for cure and post cure of HCA-SGS are presented in Fig. 9A and B, respectively, as examples to demonstrate the means by which the characteristic data was obtained. From the data of both control groups in Table 2, we see that the addition of ethanol reduced ΔH_{tot}, and reduced $T_{g\infty}$ by 12 °C, indicating a reduction in epoxy crosslinking. This may be partially due to the typical dilution effects of solvents during the curing stage [34]. However, contrasting the reduced ΔH_{tot}, the increase in ΔH_{norm} implies that the ethanol also reduced the crosslinking by taking part in the matrix cure reaction and competing with the main stoichiometric epoxy/TETA reaction.

From the composite containing silver flake and graphene without SDS (HCA-SGN) in Table 2, we can see that the addition of filler substantially reduces ΔH_{norm} compared to that of the representative ethanol diluted epoxy control. In addition, the $T_{g\infty}$ was reduced by 5 °C by the addition of filler. Since it is known that silver microflake has no significant effect on $T_{g\infty}$ [34], it appears that the addition of graphene produced both of these effects. Comparing the data for composites HCA-SGN and HCA-SGS from Table 2, where the only difference is the modification of graphene by SDS, we see no change in $T_{g\infty}$. However, the addition of SDS-modified graphene does not reduce the ΔH_{norm} as much as the addition of untreated graphene did. The reduction of ΔH_{norm} may be partly due to the moiety of oxygen functionality on graphene surfaces (i.e., C=O characteristic peak of carboxylic group at 1740 cm^{-1} in Fig. 3) acting catalytically on the reactions of epoxides and amines, or the reaction of epoxides and hydroxyls (from ethanol and the epoxy autocatalytic reaction) as discussed by others [41–44]. These would lead to an unaccounted fraction of the total reaction heat being released before the sample is placed in the DSC, reducing the reported ΔH_{norm}. However, in the case of HCA-SGS, SDS would have covered a large fraction of the graphene surface, reducing the ability of graphene to act as a catalyst. This would slow the unintended reactions of the composite before it enters the DSC, increasing the fraction of enthalpy captured. However, further investigations are

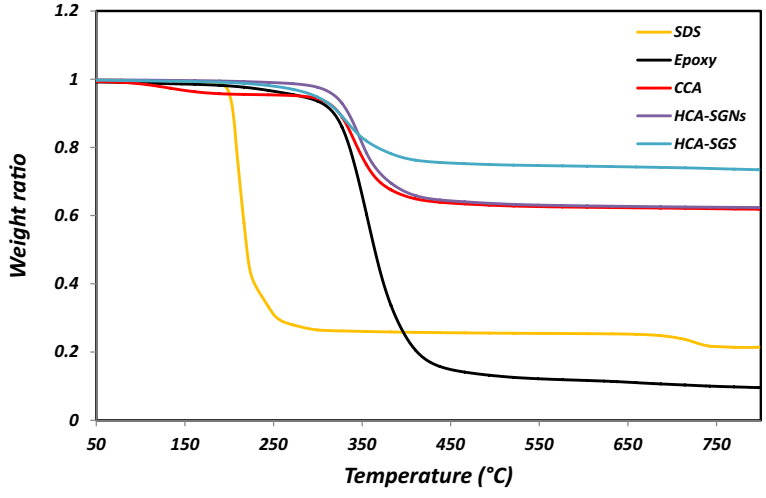

Fig. 10 – The TGA results for pure SDS, pure epoxy, the conventional ECA, hybrid ECA with non-modified graphene, and hybrid ECA with SDS-modified graphene. (A colour version of this figure can be viewed online.)

needed to clarify the exact mechanism by which the graphene and the SDS influence the reaction enthalpy.

TGA was used to characterize the thermal stability of the ECA composites. The experiment was performed for pure epoxy, pure SDS, CCA, HCA-SGN, and HCA-SGS. For all the composites, the concentration of silver flakes was 60 wt% and for the hybrid ECAs the graphene content was 1.5 wt%. As the TGA results show that pure epoxy decomposition started slowly around 300 °C, then greatly accelerated at around 325 °C (see Fig. 10). The pure SDS degraded at a much lower temperature of 200 °C. HCA-SGNs began its decomposition rapidly at approximately 325 °C, demonstrating a small but noticeable reinforcement effect from the presence of the graphene surface. HCA-SGS has a relatively lower decomposition temperature than the HCA-SGNs, perhaps because of the SDS layer between the graphene and epoxy that may weaken the reinforcement effect of graphene surface. It was noted that HCA-SGS had 12 wt% more residue after TGA degradation than the SDS-free CCA and HCA-SGN composites. This is consistent with results reported by Wang et al.; they studied composites of epoxy and SDS and observed an increase in residual wt% in the SDS-containing epoxy [45]. It is possibly due to the formation of SO_2 or a sulfonate, during SDS degradation, which would then be available to promote formation of stable char [46,47]

4. Conclusions

Graphene nanosheets with two different sizes (1 μm and 3–5 μm) were stabilized with SDS and introduced into the conventional formulation of ECAs; the effect of the graphene surface modification and its size on the electrical conductivity of ECAs was investigated. FTIR results confirmed the adsorption of SDS on graphene surface. TEM imaging confirmed the effectiveness of SDS on exfoliation of graphene nanosheets. The SDS modification of graphene decreased the percolation threshold of silver content from 40 wt% to the interestingly low value of 10 wt% while the percolation value did not change for the hybrid ECA with non-modified graphene. The electrical conductivity measurements also showed that the larger graphene is more effective in improving the electrical conductivity of ECAs and reducing the amount silver flakes than the small graphene. The bulk resistivity of HCA-LGS with 10 wt% silver flakes and 1.5 wt% graphene was 35 Ω cm while the bulk resistivity for the HCA-SGS with the same filler composition was 5.5×10^3 Ω cm. TGA and DSC experiments were performed to explore the possible effect of the SDS modification of graphene on the thermal properties of ECAs. According to DSC results, additions of both SDS-modified and unmodified graphene reduced the crosslinking of the epoxy matrix based on the reduction in T_g compared to an appropriate control group. The TGA results showed a small but noticeable reinforcement effect from the presence of the graphene surface; the SDS modification weakened this reinforcement effect.

Acknowledgements

This work was supported by a Strategic Project Grant from the Natural Sciences and Engineering Research Council of Canada (NSERC) and a Voucher for Innovation and Productivity Grant from the Ontario Centres of Excellence (OCE), Canada. We thank Mr. Andreas Korinek from Canadian Center for Electron Microscopy, McMaster University for help with TEM observation.

Appendix A. Supplementary data

Supplementary data associated with this article can be found, in the online version, at http://dx.doi.org/10.1016/j.carbon.2015.04.039.

REFERENCES

[1] Zhang R, Lin W, Moon K, Wong CP. Fast preparation of printable highly conductive polymer nanocomposites by thermal decomposition of silver carboxylate and sintering of silver nanoparticles. ACS Appl Mater Interfaces 2010;2:2637–45.
[2] Wang SJ, Geng Y, Zheng Q, Kim J-K. Fabrication of highly conducting and transparent graphene films. Carbon N Y 2010;48:1815–23.
[3] Li Z, Zhang R, Moon KS, Liu Y, Hansen K, Le T, et al. Highly conductive, flexible, polyurethane-based adhesives for flexible and printed electronics. Adv Funct Mater 2013;23:1459–65.
[4] Li Y, Moon K, Wong CP. Electronics without lead. Science 2005;308:1419–20.
[5] Meschi Amoli B, Gumfekar S, Hu A, Zhou YN, Zhao B. Thiocarboxylate functionalization of silver nanoparticles: effect of chain length on the electrical conductivity of nanoparticles and their polymer composites. J Mater Chem 2012;22:20048–56.
[6] Jiang H, Moon K, Li Y, Wong CP. Surface functionalized silver nanoparticles for ultrahigh conductive polymer composites. Chem Mater 2006;18:2969–73.
[7] Jeong W, Nishikawa H, Itou D, Takemoto T. Electrical characteristics of a new class of conductive adhesive. Mater Trans 2005;46:2276–81.
[8] Jiang H, Moon K, Lu J. Conductivity enhancement of nano silver-filled conductive adhesives by particle surface functionalization. J Electron Mater 2005;34:1432–9.
[9] Meschi Amoli B, Marzbanrad E, Hu A, Zhou YN, Zhao B. Electrical conductive adhesives enhanced with high-aspect-ratio silver nanobelts. Macromol Mater Eng 2014;299:739–47.
[10] Zhang R, Moon K, Lin W, Agar JC, Wong CP. A simple, low-cost approach to prepare flexible highly conductive polymer composites by in situ reduction of silver carboxylate for flexible electronic applications. Compos Sci Technol 2011;71:528–34.
[11] Long Y, Wu J, Wang H, Zhang X, Zhao N, Xu J. Rapid sintering of silver nanoparticles in an electrolyte solution at room temperature and its application to fabricate conductive silver films using polydopamine as adhesive layers. J Mater Chem 2011;21:4875–81.
[12] Oh Y, Chun KY, Lee E, Kim YJ, Baik S. Functionalized nano-silver particles assembled on one-dimensional nanotube scaffolds for ultra-highly conductive silver/polymer composites. J Mater Chem 2010;20:3579–82.
[13] Luan VH, Tien HN, Cuong TV, Kong B, Chung JS, Kim EJ, et al. Novel conductive epoxy composites composed of 2-D chemically reduced graphene and 1-D silver nanowire hybrid fillers. J Mater Chem 2012;22:8649.

[14] Wu HP, Liu JF, Wu XJ, Ge MY, Wang YW, Zhang GQ, et al. High conductivity of isotropic conductive adhesives filled with silver nanowires. Int J Adhes Adhes 2006;26:617–21.
[15] Chun KY, Oh Y, Rho J, Ahn JH, Kim YJ, Choi HR, et al. Highly conductive, printable and stretchable composite films of carbon nanotubes and silver. Nat Nanotechnol 2010;5:853–7.
[16] Ma R, Kwon S, Zheng Q, Kwon HY, Kim JIL, Choi HR, et al. Carbon-nanotube/silver networks in nitrile butadiene rubber for highly conductive flexible adhesives. Adv Mater 2012;24:3344–9.
[17] Stankovich S, Dikin Da, Dommett GHB, Kohlhaas KM, Zimney EJ, Stach Ea, et al. Graphene-based composite materials. Nature 2006;442:282–6.
[18] Loh KP, Bao Q, Ang PK, Yang J. The chemistry of graphene. J Mater Chem 2010;20:2277–89.
[19] Georgakilas V, Otyepka M, Bourlinos AB, Chandra V, Kim N, Kemp KC, et al. Functionalization of graphene: covalent and non-covalent approaches, derivatives and applications. Chem Rev 2012;112:6156–214.
[20] Liu K, Liu L, Luo Y, Jia D. One-step synthesis of metal nanoparticle decorated graphene by liquid phase exfoliation. J Mater Chem 2012;22:20342–52.
[21] Pu NW, Peng YY, Wang PC, Chen CY, Shi JN, Liu Y-M, et al. Application of nitrogen-doped graphene nanosheets in electrically conductive adhesives. Carbon N Y 2014;67:449–56.
[22] Bao C, Guo Y, Song L, Kan Y, Qian X, Hu Y. In situ preparation of functionalized graphene oxide/epoxy nanocomposites with effective reinforcements. J Mater Chem 2011;21:13290–8.
[23] Kim H, Miura Y, Macosko CW. Graphene/polyurethane nanocomposites for improved gas barrier and electrical conductivity. Chem Mater 2010;22:3441–50.
[24] Kim J, Yim B, Kim J, Kim J. The effects of functionalized graphene nanosheets on the thermal and mechanical properties of epoxy composites for anisotropic conductive adhesives (ACAs). Microelectron Reliab 2012;52:595–602.
[25] Tkalya EE, Ghislandi M, de With G, Koning CE. The use of surfactants for dispersing carbon nanotubes and graphene to make conductive nanocomposites. Curr Opin Colloid Interface Sci 2012;17:225–32.
[26] Pasricha R, Gupta S, Srivastava AK. A facile and novel synthesis of Ag-graphene-based nanocomposites. Small 2009;5:2253–9.
[27] Liu K, Chen S, Luo Y, Jia D, Gao H, Hu G, et al. Edge-functionalized graphene as reinforcement of epoxy-based conductive composite for electrical interconnects. Compos Sci Technol 2013;88:84–91.
[28] Peng X, Tan F, Wang W, Qiu X, Sun F, Qiao X, et al. Conductivity improvement of silver flakes filled electrical conductive adhesives via introducing silver–graphene nanocomposites. J Mater Sci Mater Electron 2014;25:1149–55.
[29] Meschi Amoli B, Trinidad J, Hu A, Zhou YN, Zhao B. Highly electrically conductive adhesives using silver nanoparticle (Ag NP)-decorated graphene: the effect of NPs sintering on the electrical conductivity improvement. J Mater Sci Mater Electron 2015;26:590–600.
[30] Lotya M, King PJ, Khan U, De S, Coleman JN. High-concentration, surfactant-stabilized graphene dispersions. ACS Nano 2010;4:3155–62.
[31] Si Y, Samulski ET. Synthesis of water soluble graphene. Nano Lett 2008;8:1679–82.
[32] Yu A, Roes I, Davies A, Chen Z. Ultrathin, transparent, and flexible graphene films for supercapacitor application. Appl Phys Lett 2010;96:253105.
[33] Davies A, Audette P, Farrow B, Hassan F, Chen Z, Choi J-Y, et al. Graphene-based flexible supercapacitors: pulse-electropolymerization of polypyrrole on free-standing graphene films. J Phys Chem C 2011;115:17612–20.
[34] Rivers G, Rogalsky A, Lee-Sullivan P, Zhao B. Thermal analysis of epoxy-based nanocomposites: have solvent effects been overlooked? J Therm Anal Calorim 2015;119. 797-05.
[35] Marcano DC, Kosynkin DV, Berlin JM, Sinitskii A, Sun Z, Slesarev A, et al. Improved synthesis of graphene oxide. ACS Nano 2010;4:4806–14.
[36] Wojtoniszak M, Rogińska D, Machaliński B, Drozdzik M, Mijowska E. Graphene oxide functionalized with methylene blue and its performance in singlet oxygen generation. Mater Res Bull 2013;48:2636–9.
[37] Viana RB, da Silva ABF, Pimentel AS. Infrared spectroscopy of anionic, cationic, and zwitterionic surfactants. Adv Phys Chem 2012;2012:1–14.
[38] Liu K, Chen S, Luo Y, Jia D, Gao H, Hu G, et al. Noncovalently functionalized pristine graphene/metal nanoparticle hybrid for conductive composites. Compos Sci Technol 2014;94:1–7.
[39] O'Neill A, Khan U, Nirmalraj PN, Boland J, Coleman JN. Graphene dispersion and exfoliation in low boiling point solvents. J Phys Chem C 2011;115:5422–8.
[40] Yang C, Wong CP, Yuen MMF. Printed electrically conductive composites: conductive filler designs and surface engineering. J Mater Chem C 2013;1:4052–69.
[41] Qiu SL, Wang CS, Wang YT, Liu CG, Chen XY, Xie HF, et al. Effects of graphene oxides on the cure behaviors of a tetrafunctional epoxy resin. Express Polym Lett 2011;5:809–18.
[42] Boukhvalov DW, Dreyer DR, Bielawski CW, Son YW. A computational investigation of the catalytic properties of graphene oxide: exploring mechanisms by using DFT methods. ChemCatChem 2012;4:1844–9.
[43] Parker RE, Isaacs NS. Mechanisms of epoxide reactions. Chem Rev 1959;59:737–99.
[44] Yang H, Shan C, Li F, Zhang Q, Han D, Niu L. Convenient preparation of tunably loaded chemically converted graphene oxide/epoxy resin nanocomposites from graphene oxide sheets through two-phase extraction. J Mater Chem 2009;19:8856.
[45] Wang W, Lu H, Liu Y, Leng J. Sodium dodecyl sulfate/epoxy composite: water-induced shape memory effect and its mechanism. J Mater Chem A 2014;2:5441.
[46] Patterson JM, Kortylewicz Z, Smith WT. Thermal degradation of sodium dodecyl sulfate. J Agric Food Chem 1984;32:782–4.
[47] Chiu YC, Chou IC, Tseng WC, Ma CCM. Preparation and thermal properties of diglycidylether sulfone epoxy. Polym Degrad Stab 2008;93:668–76.